# Reflected Shock Tube Studies of High-Temperature Rate Constants for OH + $CH_4$ → $CH_3$ + $H_2O$ and $CH_3$ + $NO_2$ → $CH_3O$ + NO

**N. K. Srinivasan, M.-C. Su,† J. W. Sutherland,‡ and J. V. Michael***

*Chemistry Division, Argonne National Laboratory, Argonne, Illinois 60439*

*Received: October 25, 2004*

The reflected shock tube technique with multipass absorption spectrometric detection of OH radicals at 308 nm has been used to study the reactions OH + $CH_4$ → $CH_3$ + $H_2O$ and $CH_3$ + $NO_2$ → $CH_3O$ + NO. Over the temperature range 840−2025 K, the rate constants for the first reaction can be represented by the Arrhenius expression $k = (9.52 \pm 1.62) \times 10^{-11}$ exp[(−4134 ± 222 K)/*T*] cm$^3$ molecule$^{-1}$ s$^{-1}$. Since this reaction is important in both combustion and atmospheric chemistry, there have been many prior investigations with a variety of techniques. The present results extend the temperature range by 500 K and have been combined with the most accurate earlier studies to derive an evaluation over the extended temperature range 195−2025 K. A three-parameter expression describes the rate behavior over this temperature range, $k = (1.66 \times 10^{-18})T^{2.182}$ exp[(−1231 K)/*T*] cm$^3$ molecule$^{-1}$ s$^{-1}$. Previous theoretical studies are discussed, and the present evaluation is compared to earlier theoretical estimates. Since $CH_3$ radicals are a product of the reaction and could cause secondary perturbations in rate constant determinations, the second reaction was studied by OH radical production from the fast reactions $CH_3O$ → $CH_2O$ + H and H + $NO_2$ → OH + NO. The measured rate constant is $2.26 \times 10^{-11}$ cm$^3$ molecule$^{-1}$ s$^{-1}$ and is not dependent on temperature from 233 to 1700 K within experimental error.

## Introduction

Experimental measurements of absolute rate constants for radical−molecule reactions play an important role in understanding atmospheric[1] and combustion chemistry.[2] In particular, reactions involving the highly reactive hydroxyl radical have received a great deal of attention because they destroy organic molecules with abstractable hydrogens in the troposphere and are important chain carriers in combustion.[1,2] The reaction of OH radicals with the simplest hydrocarbon, methane

$$OH + CH_4 \rightarrow CH_3 + H_2O \qquad (1)$$

is of continuing importance since it is the most significant depletion channel for atmospheric methane at low temperatures[3] and is also a propagation reaction in methane combustion at high temperatures.[4] Because of atmospheric and combustion interest, there are 91 studies of reaction 1 listed in the current NIST database.[5] Several of these are direct measurements of thermal rate constants at temperatures below 1000 K using static reactor or flow tube methods. Dunlop and Tully,[6] who studied reaction 1 over the temperature and pressure ranges of 293−800 K and 100−300 Torr, have reported particularly accurate values. Their results are in excellent agreement with other low-temperature values from Ravishankara and co-workers,[7] Finlayson-Pitts et al.,[8] Mellouki et al.,[9] Saunders et al.,[10] Bonard et al.,[11] and Bryukov et al.[12]

Direct high-temperature ($T$ > 1000 K) experimental rate determinations are more limited. Following the early work of Ernst et al. (1140−1505 K),[13] the most recent and reliable direct measurements are those of Felder and Madronich,[14] who studied reaction 1 over a temperature range of 298−1512 K using the flash photolysis−resonance fluorescence (FP−RF) technique. Bott and Cohen[15] later supplied a direct shock tube measurement but only at a single temperature, 1200 K. Felder and Madronich compared their results with other existing data from Jeong and Kaufman (268−473 K)[16] and Tully and Ravishankara (298−1021 K)[17] and developed a combined rate coefficient evaluation (cm$^3$ molecule$^{-1}$ s$^{-1}$):

$$k_1 = (9.50 \times 10^{-18})T^{1.96} \exp[(-1328\ \mathrm{K})/T] \qquad (2)$$

All other previously reported high-temperature measurements were deduced from flame studies[18−23] where perturbations due to secondary reactions can interfere with the primary reaction.

The lack of direct measurements at temperatures above ∼1500 K supplies the motivation for the present study. We described earlier a long absorption path multipass optical system for OH radical detection in the reflected shock regime[24] and used it to measure high-temperature rate constants.[25] In this work we have increased the path length for absorption by using 20 and 32 passes (corresponding to 1.749 and 2.798 m, respectively) as compared to 12 passes (1.049 m) in our earlier work.[24] Hence, high sensitivity for OH radical detection is possible, thereby minimizing the effects of secondary reaction perturbations; however, one potential interfering reaction could be

$$CH_3 + NO_2 \rightarrow CH_3O + NO \qquad (3)$$

since $CH_3$ radicals are formed in reaction 1. Using $CH_3I$−$NO_2$ mixtures, we therefore measured rate constants for reaction 3 by observing OH radical formation rates from the subsequent fast reactions $CH_3O$ → $CH_2O$ + H and H + $NO_2$ → OH +

* To whom correspondence should be addressed. Phone: (630) 252-3171. Fax: (630) 252-4470. E-mail: jmichael@anl.gov.

† Faculty Research Participant, Department of Educational Programs, Argonne National Laboratory. Permanent address: Department of Chemistry, Butler University, Indianapolis, IN 46208.

‡ Present address: Guest Scientist, Department of Energy and Technology, Brookhaven National Laboratory, Upton, NY 11973.

10.1021/jp040679j CCC: $30.25 
Published on Web 02/15/2005

NO. These are the first such measurements on reaction 3 at high temperatures.

## Experimental Section

The present experiments were performed with the shock tube technique using OH radical electronic absorption detection. The method and the apparatus currently being used have been previously described,[26,27] and only a brief description of the experiment will be presented here.

The shock tube is constructed from 304 stainless steel in three sections. The first 10.2 cm o.d. cylindrical section is separated from the He driver chamber by a 4 mil unscored 1100-H18 aluminum diaphragm. A 0.25 m transition section then connects the first and third sections. The third section is of rounded corner (radius 1.71 cm) square design and is fabricated from flat stock (3 mm) with a mirror finish. Two sets of flat fused silica windows (3.81 cm) with broad-band antireflection (BB AR) coating for UV light are mounted on the tube across from one another at a distance of 6 cm from the end plate. The path length between the windows is 8.745 cm. The incident shock velocity is measured with eight fast pressure transducers (PCB Piezotronics, Inc., model 113A21) mounted along the third portion of the shock tube, and temperature and density in the reflected shock wave regime are calculated from this velocity and include corrections for boundary layer perturbations.[28−30] The tube is routinely pumped between experiments to $<10^{-8}$ Torr by an Edwards Vacuum Products model CR100P packaged pumping system. A 4094C Nicolet digital oscilloscope was used to record both the velocity and absorption signals.

The optical configuration consists of an OH resonance lamp,[24,25] multipass reflectors, an interference filter at 308 nm, and a photomultiplier tube (1P28), all mounted external to the shock tube as described previously.[24,25,31] The OH lamp was constructed from a 6.4 mm o.d. Pyrex tube. High-purity Ar at atmospheric pressure was bubbled through distilled water in a glass trap, and the mixture was then introduced through a needle valve into the low-pressure (∼25 Torr) lamp. The microwave discharge was operated at 70 W. At the entrance to the multipass cell, the resultant OH resonance radiation was collimated with a set of lenses and was focused onto the reflector on the opposite side of the shock tube through two AR-coated windows that were flush mounted to the inside of the shock tube. The reflectors and windows were obtained from the CVI Laser Corp. These reflectors were attached to adjustable mounts, and the center points of the windows and mirrors were all in a coaxial position. With this new configuration, we were able to obtain either 20 or 32 passes giving total path lengths of 1.749 or 2.798 m, respectively, thereby amplifying the measured absorbances. Thus, a substantially better sensitivity (at least a factor of 2) is achieved for OH radical detection than in the previous work.[24,25]

**Gases.** High-purity He (99.995%), used as the driver gas, was from AGA Gases. Scientific grade Kr (99.999%), the diluent gas in reactant mixtures, was from Spectra Gases, Inc. The ∼10 ppm impurities ($N_2$, 2 ppm; $O_2$, 0.5 ppm; Ar, 2 ppm; $CO_2$, 0.5 ppm; $H_2$, 0.5 ppm; $CH_4$, 0.5 ppm; $H_2O$, 0.5 ppm; Xe, 5 ppm; $CF_4$, 0.5 ppm) are all either inert or in sufficiently low concentration so as to not perturb OH radical profiles. Distilled water, evaporated at 1 atm into ultra-high-purity grade Ar (99.999%) from AGA Gases, was used at ∼25 Torr pressure in the resonance lamp. Scientific grade $H_2$ (99.9999%) and $O_2$ (99.999%), for reaction mixtures, were obtained from MG Industries and were used without additional purification. Analytical grade $CH_3I$ (99%) and $C_2H_5I$ (99%), both from Aldrich Chemical Co. Inc., and technical grade $NO_2$ from Matheson Gas Products were all further purified by bulb-to-bulb distillations, with the middle thirds being retained. *tert*-Butyl hydroperoxide (TBH; 90%), used as a thermal source of OH radicals between ∼850 and 1300 K, was obtained from Sigma Aldrich Chemical Co. and was used as received. This compound is unstable, and therefore, an NMR analysis was carried out, giving an actual purity level of 55%. $CH_4$ was obtained as scientific grade from Phillips Hydrocarbons and was purified by bulb-to-bulb distillation, retaining only the middle third. $HNO_3$, used as a thermal source of OH at $T > \sim 1250$ K, was prepared and cold stored as a distillate from fuming nitric acid and concentrated sulfuric acid. Test gas mixtures were accurately prepared from pressure measurements using a Baratron capacitance manometer and were stored in an all-glass vacuum line. Once $HNO_3$ was incorporated into the reaction mixtures, the mixtures were stable as judged from the level of $[OH]_0$ produced in successive experiments. However, it is difficult to prepare highly purified $HNO_3$ from a single bulb-to-bulb distillation, and therefore, the mixtures undoubtedly contained small amounts of $NO_2$ and $H_2O$.

## Results

Since the multipass optical system used in this work is new, the curve-of-growth for OH radicals was determined under conditions similar to those of the anticipated kinetics experiments. The same method used previously[24] was employed. OH radicals were generated by the H + $NO_2$ reaction.[25] Known concentrations of H atoms are obtained from the thermal decomposition of $C_2H_5I$.[32]

$$C_2H_5I\ (+M) \rightarrow C_2H_5 + I\ (+M) \tag{4}$$

$$C_2H_5I\ (+M) \rightarrow C_2H_4 + HI\ (+M) \tag{5}$$

$$C_2H_5\ (+M) \rightarrow C_2H_4 + H\ (+M) \tag{6}$$

$$H + NO_2 \rightarrow OH + NO \tag{7}$$

Reaction 6 is so fast compared to reactions 4 and 5 that the thermal decomposition of $C_2H_5I$ controls the rate of formation of H. Thus, by using relatively high concentrations of $NO_2$, the rate for reaction 7 can be adjusted to be sufficiently high that a concentration pulse of OH radicals is produced over very short times compared to that of the kinetics experiment. The nearly instantaneous level of measured absorbance, $(ABS)_0 = \ln[I_0/I_t] = [OH]_0 l \sigma_{OH}$, was then correlated with $[OH]_0$ as determined from the mechanism in reactions 4−7 for known initial concentrations of $C_2H_5I$ and $NO_2$. Thirty-five experiments, ranging from 1100 to 2000 K, were carried out with varying initial reactant concentrations, and the absorption cross-section, $\sigma_{OH}$, was determined for each experiment with the measured path length used with multipass operation. The results are plotted in Figure 1 as solid blue circles. In addition, the branched chain oxidation of $H_2$ was employed to obtain $\sigma_{OH}$ values at higher temperatures, up to 3000 K, again with multipass operation. The level of [OH] produced at long times in these latter experiments was calculated from appropriate chemical simulations of the branched chain $H_2/O_2$ system. This concentration is determined totally by equilibrium constants for the propagation reactions, and as shown recently,[33] the long time prediction is now in complete agreement with the new heat of formation of OH radicals[34] that was incorporated into our simulations. We carried out 23 of these experiments, and these results are also shown in Figure 1 as solid squares. The temperature dependence

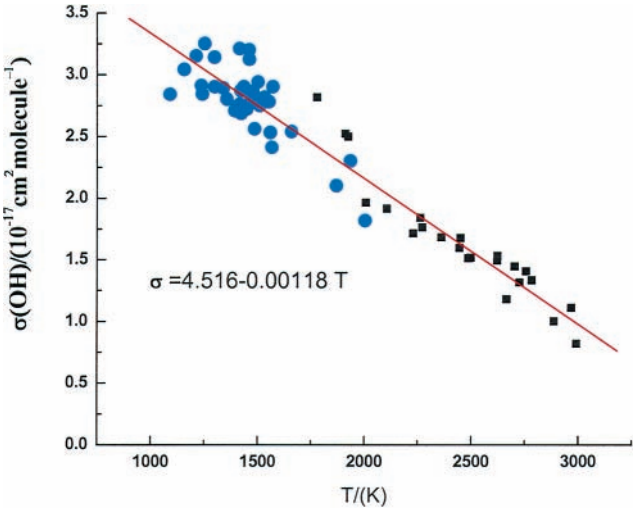


**Figure 1.** Absorption cross-section ($\sigma_{OH}$) vs temperature: (solid blue dots) $C_2H_5I/NO_2$ experiments; (■) $H_2/O_2$ experiments. The red line is the linear least-squares result, eq 8, which includes all data points.

of the combined sets is given by the linear equation

$$\sigma_{OH} = (4.516 - 0.00118T) \times 10^{-17}\ \text{cm}^2\ \text{molecule}^{-1} \quad (8)$$

and the values determined from eq 8 agree with an earlier single-pass determination from this laboratory[35] using the same technique for preparing OH, namely, reactions 4−7.

Determining absolute [OH] with eq 8, kinetics experiments for OH + $CH_4$ at $T > 1223$ K were carried out using $HNO_3$ as the thermal source of OH radicals. Table 1 gives the conditions, and in these experiments, 20 optical passes were used. Because of the difficulties in delivering known quantities of $HNO_3$, the values given for the mole fraction of nitric acid in the table are estimated and are based on the zero time extrapolation to $[OH]_0$. A typical OH profile is shown in Figure 2, where three chemical simulations are displayed as lines. In all experiments, first-order analysis was initially used to obtain an approximate value for $k_1$. The final values for $k_1$ were obtained from simulation studies that employed a 38-step mechanism (solid line in the figure), and this mechanism with rate constants and references is available as Supporting Information. The values obtained and tabulated in Table 1 are predominately determined by the OH + $CH_4$ reaction, and therefore, these results can be considered to be essentially direct measurements. This was corroborated with a linear sensitivity analysis as shown in Figure 3, where the dominant reaction, particularly during the initial stages, is reaction 1. The dashed line simulation in Figure 2 is obtained with $k_1 = 0$ and shows a slight $[OH]_t$ increase due to the thermal decomposition of $NO_2$ followed by O + $CH_4 \rightarrow$ OH + $CH_3$. The third simulation in Figure 2 was carried out with the same $k_1$ value but with a reduced mechanism consisting of the six most sensitive reactions shown in Figure 3 as the inset.

As stated in the Experimental Section, small amounts of both $NO_2$ and $H_2O$ were present in the reactant mixtures. The possible implications of these contaminants were investigated using chemical simulations in which varying amounts of both molecules were initially present. The reactions of $H_2O$ with $CH_3$, H, and O are far too slow to affect our conclusions. However, the reactions of $NO_2$ with these species are more problematic since OH can be formed from H + $NO_2$ and $CH_3$ + $NO_2$. Both reactions result in re-formation of OH at long reaction times, generating profiles that gradually tail out and in some cases appear to approach steady state. H + $NO_2$ rate constants have already been measured in this laboratory,[25] but $CH_3$ + $NO_2$ has never been directly measured at high temperature. Since this is a potentially complicating reaction, we determined the rate constants by using $CH_3I$ as a thermal source of $CH_3$ in the presence of an excess of $NO_2$. The conditions for and results of these experiments are given in Table 2. In this case, OH is produced from

$$CH_3 + NO_2 \rightarrow CH_3O + NO \quad (3)$$

$$CH_3O\ (+M) \rightarrow CH_2O + H\ (+M) \quad (9)$$

$$H + NO_2 \rightarrow OH + NO \quad (7)$$

Since reactions 9 and 7 are effectively instantaneous on the time scale of the experiment, the time dependence of [OH] formation gives a reliable value for the rate-controlling step, reaction 3. $[OH]_t$ was measured and fitted with kinetics simulations, yielding the values listed in Table 2 and plotted in Figure 4. Between 1360 and 1695 K, the rate constants are temperature-independent within experimental error, giving $k = (2.4 \pm 0.7) \times 10^{-11}$ cm$^3$ molecule$^{-1}$ s$^{-1}$. Applying both rate constants, reactions 3 and 7, in simulations to the data in Table 1 with initial $NO_2$ being present shows that perturbations due to these secondary reactions are negligible if the fits are weighted toward initial times; that is, to times less than 300−400 $\mu$s. We adopted this criterion for the rate constant analyses given in Table 1.

Data for the OH + $CH_4$ reaction were also obtained at lower temperatures using *tert*-butyl hydroperoxide (TBH), $(CH_3)_3$-COOH, as the source of OH radicals.[15] This molecule is so unstable that it decomposes almost instantaneously (eliminating the possibility of observing [OH] rise times) above ∼800 K, giving $(CH_3)_2CO$, OH, and $CH_3$.[5] Because 800 K is exceeded in the incident shock regime, for shock strengths that give 1370 K in the reflected shock regime, these experiments were limited to $T < \sim$1300 K. In this set of experiments, the optical detection system was further improved by employing 32 optical passes. A typical profile is shown in Figure 5, where the solid line represents the best fit of simulations obtained with varying values for $k_1$, but with fixed rate constants for $CH_3$ + $CH_3$,[36] OH + OH,[26,37] and $CH_3$ + OH.[38] Besides the thermal decomposition rate for TBH, these are the only important processes that affect $[OH]_t$. For the initial $[OH]_0$ used here (that is, $[TBH]_0$), the self-combinations are too slow to appreciably perturb the profile; however, the cross-combination rate constant, recently measured in this laboratory,[38] does contribute to OH decay. This is shown in Figure 5 as the dashed line, where the decrease in $[OH]_t$ with $[CH_4] = 0$ is almost entirely due to the $CH_3$ + OH reaction. This perturbation typically amounted to only ∼20% of the total decay with added $CH_4$, and therefore, the dominant reaction that affects the decay is reaction 1. Hence, the rate constants given in Table 1 for this reaction can be considered to be essentially direct.

## Discussion

Since reaction 3 might perturb the results for reaction 1, we consider it first in the discussion.

**$CH_3$ + $NO_2$.** The $CH_3$ + $NO_2$ reaction has been studied previously by Glaenzer and Troe,[39] Yamada et al.,[40] Biggs et al.,[41] Glarborg et al.,[42] and Wollenhaupt and Crowley.[43] In the earlier studies, the reported values were 2.16 (1100−1400 K),[39] 2.52 (295 K),[40] and 2.31 (298 K),[41] all in units of $10^{-11}$ cm$^3$ molecule$^{-1}$ s$^{-1}$, suggesting temperature independence over the

**TABLE 1: High-Temperature Rate Data for OH + $CH_4$ → $CH_3$ + $H_2O$**

| $P_1$/ Torr | $M_s$[a] | $\rho_5$[b]/ ($10^{18}$ cm$^{-3}$) | $T_5$[b]/ K | $k_1$[c] | $P_1$/ Torr | $M_s$[a] | $\rho_5$[b]/ ($10^{18}$ cm$^{-3}$) | $T_5$[b]/ K | $k_1$[c] |
|---|---|---|---|---|---|---|---|---|---|
| $X_{HNO_3} \approx 6.852 \times 10^{-6}$ | | $X_{CH_4} = 1.972 \times 10^{-4}$ | | | $X_{HNO_3} \approx 6.852 \times 10^{-6}$ | | $X_{CH_4} = 1.972 \times 10^{-4}$ | | |
| 15.92 | 2.412 | 2.921 | 1449 | 6.50(−12)[d] | 16.00 | 2.641 | 3.222 | 1697 | 9.00(−12) |
| 15.94 | 2.469 | 2.993 | 1511 | 7.60(−12) | 15.84 | 2.476 | 3.004 | 1509 | 7.70(−12) |
| 15.98 | 2.506 | 3.044 | 1553 | 6.47(−12) | 15.84 | 2.468 | 2.994 | 1500 | 6.24(−12) |
| 15.94 | 2.560 | 3.099 | 1615 | 7.97(−12) | 10.91 | 2.685 | 2.239 | 1756 | 8.30(−12) |
| 15.94 | 2.528 | 3.062 | 1578 | 7.26(−12) | 10.94 | 2.668 | 2.232 | 1736 | 7.50(−12) |
| $X_{HNO_3} \approx 1.435 \times 10^{-5}$ | | $X_{CH_4} = 1.873 \times 10^{-4}$ | | | $X_{HNO_3} \approx 1.435 \times 10^{-5}$ | | $X_{CH_4} = 1.873 \times 10^{-4}$ | | |
| 10.91 | 2.631 | 2.199 | 1692 | 9.15(−12) | 10.89 | 2.507 | 2.099 | 1549 | 7.00(−12) |
| 10.87 | 2.433 | 2.034 | 1467 | 5.50(−12) | 10.90 | 2.667 | 2.223 | 1734 | 7.60(−12) |
| 10.95 | 2.686 | 2.248 | 1757 | 7.50(−12) | | | | | |
| $X_{HNO_3} \approx 7.121 \times 10^{-6}$ | | $X_{CH_4} = 3.955 \times 10^{-4}$ | | | $X_{HNO_3} \approx 7.121 \times 10^{-6}$ | | $X_{CH_4} = 3.955 \times 10^{-4}$ | | |
| 15.94 | 2.332 | 2.832 | 1358 | 4.37(−12) | 10.93 | 2.315 | 1.936 | 1346 | 5.66(−12) |
| 10.93 | 2.430 | 2.035 | 1468 | 5.40(−12) | 10.89 | 2.458 | 2.051 | 1499 | 7.59(−12) |
| 10.91 | 2.327 | 1.943 | 1359 | 5.34(−12) | 15.93 | 2.393 | 2.909 | 1424 | 5.82(−12) |
| 10.97 | 2.278 | 1.909 | 1308 | 4.91(−12) | 16.00 | 2.296 | 2.796 | 1321 | 4.51(−12) |
| 10.88 | 2.452 | 2.045 | 1493 | 6.69(−12) | 15.91 | 2.199 | 2.648 | 1223 | 3.47(−12) |
| 10.95 | 2.218 | 1.850 | 1247 | 3.19(−12) | 15.84 | 2.279 | 2.736 | 1308 | 3.80(−12) |
| 10.91 | 2.359 | 1.971 | 1392 | 5.95(−12) | 15.78 | 2.324 | 2.794 | 1350 | 4.85(−12) |
| 10.97 | 2.396 | 2.014 | 1432 | 6.64(−12) | | | | | |
| $X_{HNO_3} \approx 8.700 \times 10^{-6}$ | | $X_{CH_4} = 1.388 \times 10^{-4}$ | | | $X_{HNO_3} \approx 8.700 \times 10^{-6}$ | | $X_{CH_4} = 1.388 \times 10^{-4}$ | | |
| 10.90 | 2.548 | 2.104 | 1618 | 6.40(−12) | 15.91 | 1.701 | 3.230 | 1791 | 8.70(−12) |
| 10.97 | 2.765 | 2.284 | 1872 | 9.40(−12) | 15.99 | 2.816 | 3.369 | 1931 | 1.10(−11) |
| 10.84 | 2.716 | 2.220 | 1815 | 1.21(−11) | 16.00 | 2.842 | 3.395 | 1964 | 1.20(−11) |
| 10.85 | 2.638 | 2.166 | 1720 | 7.70(−12) | 15.93 | 2.663 | 3.204 | 1738 | 6.00(−12) |
| 10.92 | 2.788 | 2.290 | 1902 | 9.10(−12) | 15.89 | 2.750 | 3.276 | 1851 | 7.94(−12) |
| 10.98 | 2.739 | 2.276 | 1834 | 9.10(−12) | 15.86 | 2.705 | 3.230 | 1793 | 7.50(−12) |
| 10.94 | 2.884 | 2.357 | 2025 | 1.30(−11) | 15.94 | 2.805 | 3.341 | 1920 | 9.95(−12) |
| 15.97 | 2.576 | 3.113 | 1639 | 6.50(−12) | | | | | |
| $X_{tert-butyl-HP} = 1.630 \times 10^{-5}$ | | $X_{CH_4} = 6.113 \times 10^{-4}$ | | | $X_{tert-butyl-HP} = 1.630 \times 10^{-5}$ | | $X_{CH_4} = 6.113 \times 10^{-4}$ | | |
| 10.98 | 2.024 | 1.638 | 1071 | 1.50(−12) | 15.93 | 1.882 | 2.135 | 947 | 9.00(−13) |
| 10.83 | 2.094 | 1.686 | 1142 | 3.00(−12) | 15.94 | 1.753 | 1.926 | 840 | 7.00(−13) |
| 10.92 | 2.109 | 1.716 | 1157 | 2.50(−12) | 15.92 | 1.870 | 2.115 | 937 | 1.10(−12) |
| 11.02 | 2.195 | 1.824 | 1235 | 3.50(−12) | 15.85 | 1.972 | 2.281 | 1020 | 1.70(−12) |
| 10.89 | 2.076 | 1.684 | 1122 | 2.30(−12) | 15.88 | 2.059 | 2.417 | 1101 | 3.10(−12) |
| 10.98 | 1.975 | 1.587 | 1031 | 1.20(−12) | 15.96 | 2.170 | 2.588 | 1206 | 3.20(−12) |
| 10.95 | 1.888 | 1.489 | 954 | 1.20(−12) | 15.94 | 1.823 | 2.055 | 891 | 8.00(−13) |
| 10.92 | 1.845 | 1.432 | 920 | 1.10(−12) | 15.94 | 2.100 | 2.486 | 1139 | 2.60(−12) |
| 10.92 | 1.857 | 1.446 | 931 | 1.00(−12) | 15.93 | 2.141 | 2.544 | 1179 | 3.40(−12) |
| 15.88 | 1.952 | 2.240 | 1010 | 1.80(−12) | 14.57 | 2.233 | 2.447 | 1271 | 3.80(−12) |

[a] The error in measuring the Mach number, $M_s$, is typically 0.5−1.0% at the 1 standard deviation level. [b] Quantities with the subscript 5 refer to the thermodynamic state of the gas in the reflected shock region. [c] Rate constants in units of cm$^3$ molecule$^{-1}$ s$^{-1}$. [d] Parentheses denote the power of 10.

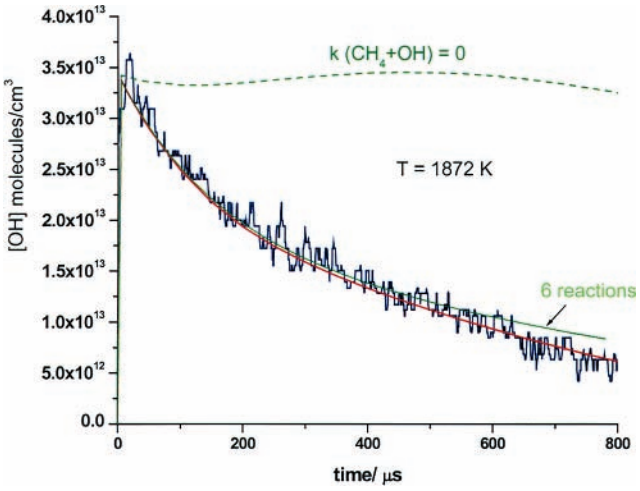


**Figure 2.** Sample temporal profile of OH absorption: solid red line, fit with the full reaction mechanism; green dashed line, simulation with $k_1 = 0$. The solid green line is a simulation with only six reactions (see the text). $P_1 = 10.97$ Torr, $M_s = 2.765$, $T_5 = 1872$ K, $\rho_5 = 2.284 \times 10^{18}$ molecules cm$^{-3}$, $[HNO_3]_0 \approx 3.4 \times 10^{13}$ molecules cm$^{-3}$, and $[CH_4]_0 = 3.170 \times 10^{14}$ molecules cm$^{-3}$.

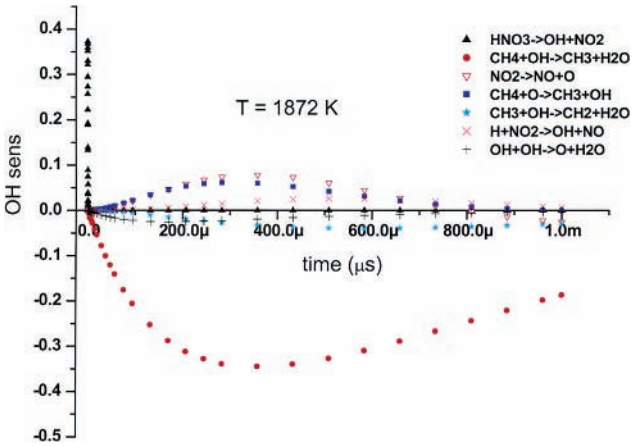


**Figure 3.** OH radical sensitivity analysis for the profile shown in Figure 2 using the full reaction mechanism scheme and the final fitted values of $k_1 = 9.4 \times 10^{-12}$ cm$^3$ molecule$^{-1}$ s$^{-1}$. The seven most sensitive reactions are shown.

range 295−1400 K. However, Glarborg et al.[42] reinvestigated the existing data[39,44,45] on the thermal decomposition of $CH_3$-$NO_2$ and, including the lower $T$ determinations,[40,41] concluded that $k_3 = (6.6 \times 10^{-11})T^{-0.2}$ cm$^3$ molecule$^{-1}$ s$^{-1}$.

Yamaguchi et al.[46] have carried out electronic structure calculations on the $CH_3 + NO_2$ interaction and have shown that there are two possible reaction pathways, one through ni-

**TABLE 2: High-Temperature Rate Data for $CH_3 + NO_2 \rightarrow CH_3O + NO$**

| $P_1$/ Torr | $M_s$[a] | $\rho_5$[b]/ ($10^{18}$ cm$^{-3}$) | $T_5$[b]/ K | $k_3$[c] |
|---|---|---|---|---|
| $X_{CH_3I} = 1.048 \times 10^{-5}$ | | $X_{NO_2} = 1.256 \times 10^{-4}$ | | |
| 15.95 | 2.443 | 2.944 | 1493 | 3.00(−11)[d] |
| 10.98 | 2.590 | 2.152 | 1666 | 1.70(−11) |
| 10.99 | 2.582 | 2.148 | 1657 | 2.20(−11) |
| 10.91 | 2.402 | 1.988 | 1454 | 3.50(−11) |
| 10.98 | 2.574 | 2.154 | 1637 | 2.00(−11) |
| 10.95 | 2.536 | 2.112 | 1599 | 3.00(−11) |
| 10.95 | 2.322 | 1.932 | 1363 | 3.00(−11) |
| 10.92 | 2.618 | 2.169 | 1694 | 1.40(−11) |
| 10.89 | 2.447 | 2.029 | 1498 | 1.90(−11) |
| 10.93 | 2.434 | 2.025 | 1484 | 2.00(−11) |
| 10.95 | 2.488 | 2.073 | 1544 | 1.70(−11) |
| 10.89 | 2.391 | 1.981 | 1436 | 2.20(−11) |
| 10.89 | 2.419 | 2.005 | 1467 | 2.90(−11) |

[a] The error in measuring the Mach number, $M_s$, is typically 0.5−1.0% at the 1 standard deviation level. [b] Quantities with the subscript 5 refer to the thermodynamic state of the gas in the reflected shock region. [c] Rate constants in units of cm$^3$ molecule$^{-1}$ s$^{-1}$. [d] Parentheses denote the power of 10.

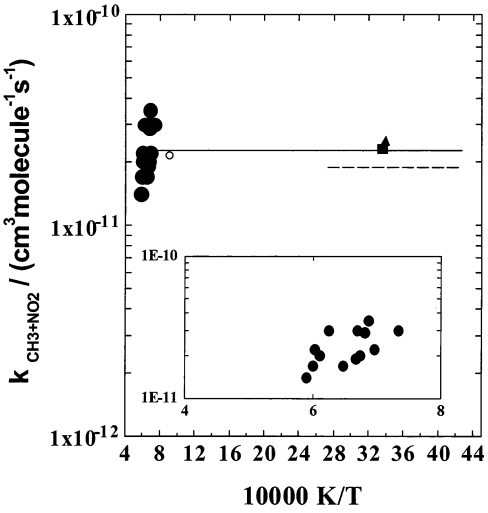


**Figure 4.** Arrhenius plot of the data for $CH_3 + NO_2$ from Table 2: (●) present work (1360−1695 K); (■) ref 40; (▲) ref 41; (○) ref 39; (solid line) average value (see the text); (dotted line) ref 43.

tromethane and the other through nitrosomethane. There is a cyclic transition state connecting the two isomeric paths; however, it is 9 kcal mol$^{-1}$ higher lying than the reactants. The products $CH_3O + NO$ lie 17 kcal mol$^{-1}$ below the reactants on the nitrosomethane surface. Hence, these products are associated with nitrosomethane, and the rate constants for this addition−elimination reaction are the high-pressure limit for this pathway. The nitromethane pathway can only give stabilized $CH_3NO_2$ and will therefore be pressure dependent.

Using LIF detection of $CH_3O$, the pathway through nitromethane has recently been studied by Wollenhaupt and Crowley,[43] who measured the pressure and temperature dependences of the rate constants over the ranges 10−200 Torr and 233−356 K. They found it necessary to invoke a temperature-independent low-pressure rate constant of $1.91 \times 10^{-11}$ cm$^3$ molecule$^{-1}$ s$^{-1}$, to be associated with the nitrosomethane addition−elimination path, reaction 3.

The question arises as to whether the pressure-dependent nitromethane path contributes to the overall rate in both the present and earlier work. Wollenhaupt and Crowley[43] fitted their data with an empirical Troe model and then applied it to the previous low-temperature and -pressure results. We have also applied their model for the conditions shown in Table 2 and find ∼20% contribution. However, this conclusion is not firm since the extrapolation is long (∼300−1700 K), the fitting procedure is approximate, and an invariant $F_{cent}$ value is used in the model. Hence, we conclude that the present and earlier results along with the low-pressure value from Wollenhaupt and Crowley are measurements of $k_3$. Within experimental error, a strong temperature dependence between 233 and 1700 K is not indicated, and we therefore, recommend the average value from the present and all previous[39−43] studies, $k_3 = 2.26 \times 10^{-11}$ cm$^3$ molecule$^{-1}$ s$^{-1}$, as shown in Figure 4. Use of this value in the mechanism for $k_1$ determination shows that it is negligibly slow as seen in the sensitivity analysis of Figure 3.

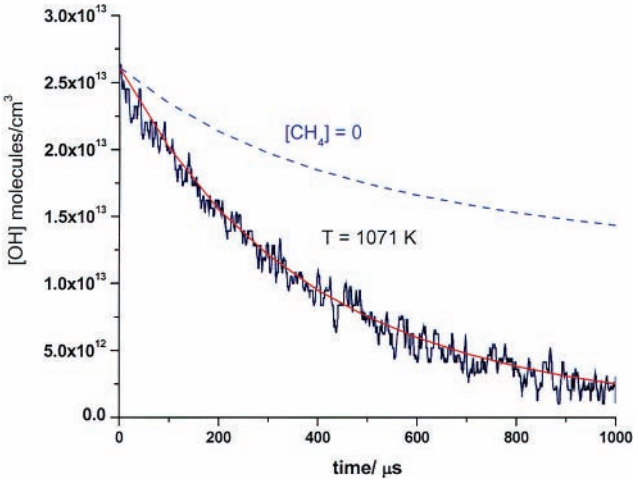


**Figure 5.** Sample temporal profile of OH absorption at low $T$ using TBH, $(CH_3)_3COOH$, as the source for OH radicals: solid red line, see the text; blue dashed line, simulation with $[CH_4]_0 = 0$. $P_1 = 10.98$ Torr, $M_s = 2.024$, $T_5 = 1071$ K, $\rho_5 = 1.638 \times 10^{18}$ molecules cm$^{-3}$, $[(CH_3)_3COOH]_0 = 2.670 \times 10^{13}$ molecules cm$^{-3}$, and $[CH_4]_0 = 1.001 \times 10^{15}$ molecules cm$^{-3}$.

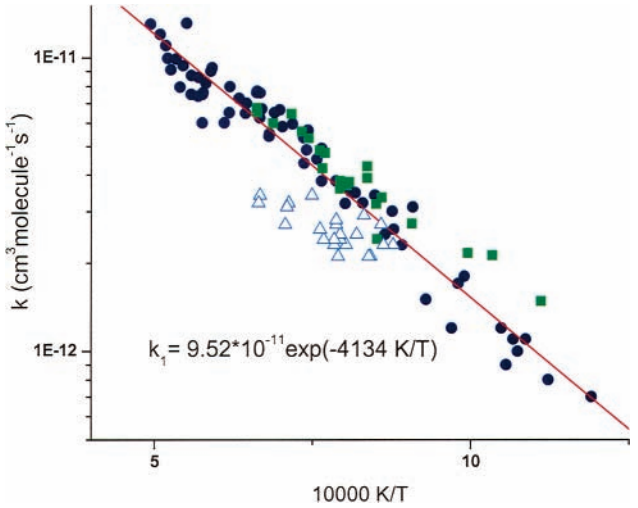


**Figure 6.** Arrhenius plot of the data from Table 1. The red line is the linear least-squares result, eq 10, which includes all of the present data points. Also shown are data from (blue triangles) ref 13 and (green squares) ref 14.

**OH + $CH_4$.** The rate constant results of Table 1 are plotted in Figure 6 in Arrhenius form. The data can be represented in cm$^3$ molecule$^{-1}$ s$^{-1}$ with a 2 standard deviation error by the linear least-squares expression

$$k_1 = (9.52 \pm 1.62) \times 10^{-11} \exp[(-4134 \pm 222\ \text{K})/T] \quad (10)$$

Equation 10 is plotted as the solid line in the figure and is

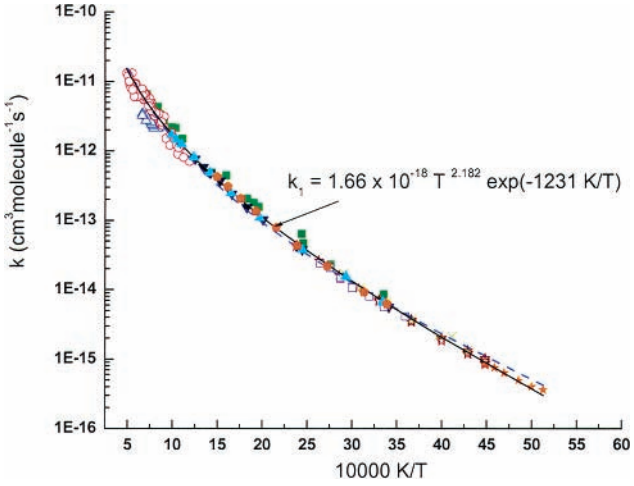


**Figure 7.** Arrhenius plot for $CH_4 + OH$: (○) present work; (green squares) ref 14; (open triangles) ref 13; (blue inverted triangles) ref 6; (open stars) ref 7; (solid orange stars) ref 7; (green crosses) ref 9; (open squares) ref 8; (solid blue triangles) ref 12; (solid orange pentagons) ref 11; (black solid line) eq 11; (blue dashed line) eq 12 (see the text).

applicable over the temperature range 840−2025 K. Therefore, the database for reaction 1 has been increased by ∼500 K over that attained by Ernst et al.[13] and Madronich and Felder,[14] whose results are ∼9−12% lower and ∼12−60% higher than eq 10, respectively, as seen in Figure 6.

The present results are compared to earlier data in Figure 7. In addition to the two high-temperature studies,[13,14] particularly accurate lower temperature studies are also included in the figure.[6−9,11,12] An evaluation for $k_1$ that gives equal weight to each study was carried out using the reported rate constant expressions from each of the studies to determine a database. Over equal increments of $T^{-1}$, five points were calculated from each expression, but only over the $T$ range of the given study. Including the present result, eq 10, the database then consisted of 45 points, and a three-parameter nonlinear least-squares expression of the form $k = AT^n \exp(-B/T)$ was derived. Over the $T$ range 195−2025 K we obtain

$$k_1 = (1.66 \times 10^{-18})T^{2.182} \exp[(-1231\ \mathrm{K})/T] \qquad (11)$$

This expression is plotted as the solid line in Figure 7, where it is seen to be an excellent representation of the experimental data. All data sets lie within ±12% of this expression, with the exception of the present values at 840 and 2025 K, where the discrepancy is ∼±20%, and with the values of Madronich and Felder between 298 and 750 K, where their values (as reflected in their evaluation, eq 2) are ∼20−25% higher than eq 11.

There have been at least 14 prior theoretical investigations of reaction 1.[47−60] Cohen used a thermochemical kinetics model to estimate $k_1$.[47] However, most of these studies were primarily concerned with calculating the potential energy of interaction using ab initio methods. Given a potential energy surface, all methods for treating the dynamics (that is, conventional (CTST) or variational (VTST) transition-state theory, quasi-classical trajectory theory (QCT), or quantum scattering theory) generally predict similar nonlinear Arrhenius plots as explicitly shown using VTST in ref 60. Hence, nonlinearity is not a result of the chosen dynamics method. Rather, for a given barrier height, the dominant causes are three or four low-valued bending frequencies in the transition states (including those that correlate with hindered rotations) and tunneling factors, which all strongly contribute to the $A$ factor temperature dependence. For reaction 1, the transition-state geometry is about the same using any of the ab initio electronic structure methods, but there is substantial variability in both force fields and energies.[48−60] To illustrate this point, Truong and Truhlar, Melissas and Truhlar, Dobbs et al., and Schwartz et al. report low-valued transition-state frequencies and imaginary frequencies ($cm^{-1}$) as 57, 223, 340, 827, and 1617i,[50] 40, 316, 356, 756, and 1830i,[51] 20, 335, 339, 797, and 1724i,[52] and 43, 343, 347, 495, and 1084i,[57] respectively. All agree that there is one low frequency that correlates to an essentially free rotor, but the scaled zero-point-corrected $\Delta E_0^{\ddagger}$ values, which are moderately successful in explaining the magnitude of $k_1$, are 6.6, 5.9, 5.2, and 6.5 kcal $mol^{-1}$, respectively. The energy scaled values are also dependent on both the magnitude of the imaginary frequency (ranging from 1084i to 1830i $cm^{-1}$) and the method used to calculate the tunneling factors. Hence, the "successful" calculations are balanced among all these factors.

With a clear understanding of the issues raised above, Espinosa-Garcia and Corchado[59] calibrated these factors to obtain agreement with experimental data. They carried out canonical unified statistical variational transition-state theoretical calculations with microcanonical optimized multidimensional tunneling factors included. They constructed a reaction pathway, force field, and energetics that fitted existing experimental data quite accurately. The low-valued transition-state frequencies and imaginary frequency ($cm^{-1}$) from this procedure are 34, 432, 440, 630, and 1703i,[59] and the zero-point-corrected $\Delta E_0^{\ddagger}$ is 4.9 kcal $mol^{-1}$. Over the temperature range 200−2000 K, their computed results can be represented to within ±6% by the three-parameter expression

$$k_1 = (2.52 \times 10^{-20})T^{2.724} \exp[(-905\ \mathrm{K})/T] \qquad (12)$$

Equation 12 is plotted as the dashed line in Figure 7, where the agreement between the present evaluation, eq 11, and eq 12 is seen to be excellent. These two equations are within ±15% of one another over the range 250−2000 K, with eq 12 diverging only at 195 K to a value 40% higher than that of eq 11.

Despite the excellent agreement noted above, it would be premature to presume that theory is complete on this reaction. New higher level calculations of the potential energy surface are clearly needed. Masgrau et al.[60] have both increased the level of electronic structure calculations and have extended the VTST methods in an attempt to calculate isotope effects, but with only moderate success. It is probable that the differences are due to the various methods adopted for tunneling corrections. It may be that direct quantum scattering calculations might give a more realistic description of tunneling. Nyman and Clary[54] have already carried out such calculations for $k_1$ using approximate potential energy surfaces. One of the surfaces gave results that agreed relatively well with experiment. Using a more accurate potential energy surface for $H + CH_4$, Kerkeni and Clary[61] have recently described a new procedure for performing quantum-dynamical calculations that agreed well with existing experiments. With a more accurate ab initio potential energy surface for $OH + CH_4$, it would be interesting to test whether such an approach would give a superior theoretical description for $k_1$.

**Acknowledgment.** This work was supported by the U.S. Department of Energy, Office of Basic Energy Sciences, Division of Chemical Sciences, Geosciences and Biosciences, under Contract No. W-31-109-Eng-38.

**Supporting Information Available:** Table of mechanism for fitting [OH] profiles for $CH_4 + OH$. This material is available free of charge via the Internet at http://pubs.acs.org.

## References and Notes


(1) DeMore, W. B.; Sander, S. P.; Golden, D. M.; Hampson, R. F.; Kurylo, M. J.; Howard, C. J.; Ravishankara, A. R.; Kolb, C. E.; Molina, M. J. *Chemical Kinetics and Photochemical Data for Use in Stratospheric Modeling*; Evaluation No. 12, JPL Publication 97-4; Jet Propulsion Laboratory: Pasadena, CA, 1997.

(2) Warnatz, J. In *Combustion Chemistry*; Gardiner, W. C., Jr., Ed.; Springer-Verlag: New York, 1984; p 197.

(3) Wayne, R. P. *Chemistry of Atmospheres*; Clarendon Press: Oxford, 1985; p 22.

(4) Hwang, S. M.; Ryu, S.-O.; De Witt, K. J.; Rabinowitz, M. J. *J. Phys. Chem. A* **1999**, *103*, 5949.

(5) *NIST Chemical Kinetics Database*; NIST Standard Reference Database 17; NIST: Gaithersburg, MD, 2000.

(6) Dunlop, J. R.; Tully, F. P. *J. Phys. Chem.* **1993**, *97*, 11148.

(7) Vaghjiani, G. L.; Ravishankara, A. R. *Nature* **1991**, *350*, 406. Gierczak, T.; Talukdar, R. K.; Herndon, S. C.; Vaghjiani, G. L.; Ravishankara, A. R. *J. Phys. Chem. A* **1997**, *101*, 3125.

(8) Finlayson-Pitts, B. J.; Ezell, M. J.; Jayaweera, T. M.; Berko, H. N.; Lai, C. C. *Geophys. Res. Lett.* **1992**, *19*, 1371.

(9) Mellouki, A.; Teton, S.; Laverdet, G.; Quilgars, A.; Le Bras, G. *J. Chim. Phys. Phys.-Chim. Biol.* **1994**, *91*, 473.

(10) Saunders, S. M.; Hughes, K. J.; Pilling, M. J.; Baulch, D. L.; Smurthwaite, P. I. In *Optical Methods in Atmospheric Chemistry*; Platt, H. I. S. a. U., Ed.; SPIE: Bellingham, WA, 1992; Vol. 1715, p 88.

(11) Bonard, A.; Daele, V.; Delfau, J.-L.; Vovelle, C. *J. Phys. Chem. A* **2002**, *106*, 4384.

(12) Bryukov, M. G.; Knyazev, V. D.; Lomnicki, S. M.; McFerrin, C. A.; Dellinger, B. *J. Phys. Chem. A* **2004**, *108*, 10464.

(13) Ernst, J.; Wagner, H. Gg.; Zellner, R. *Ber. Bunsen-Ges. Phys. Chem.* **1978**, *82*, 409.

(14) Madronich, S.; Felder, W. *Proc. Combust. Inst.* **1984**, *20*, 703, Felder, W.; Madronich, S. *Combust. Sci. Technol.* **1986**, *50*, 135.

(15) Bott, J. F.; Cohen, N. *Int. J. Chem. Kinet.* **1989**, *21*, 485.

(16) Jeong, K. M.; Kaufman, F. *J. Phys. Chem.* **1982**, *86*, 1808.

(17) Tully, F. P.; Ravishankara, A. R. *J. Phys. Chem.* **1980**, *84*, 3126.

(18) Dixon-Lewis, G.; Williams, A. *Proc. Combust. Inst.* **1967**, *11*, 951.

(19) Peeters, J.; Mahnen, G. *Proc. Combust. Inst.* **1973**, *14*, 133.

(20) Fenimore, C. P.; Jones, G. W. *J. Phys. Chem.* **1961**, *65*, 2200.

(21) Westenberg, A. A.; Fristrom, R. M. *J. Phys. Chem.* **1961**, *65*, 591.

(22) Fristrom, R. M. *Proc. Combust. Inst.* **1963**, *9*, 560.

(23) Wilson, W. E.; O'Donovan, J. T.; Fristrom, R. M. *Proc. Combust. Inst.* **1969**, *12*, 929.

(24) Su, M.-C.; Kumaran, S. S.; Lim, K. P.; Michael, J. V. *Rev. Sci. Instrum.* **1995**, *66*, 4649.

(25) Su, M.-C.; Kumaran, S. S.; Lim, K. P.; Michael, J. V.; Wagner, A. F.; Harding, L. B.; Fang, D.-C. *J. Phys. Chem. A* **2002**, *106*, 8261.

(26) Michael, J. V. *Prog. Energy Combust. Sci.* **1992**, *18*, 327.

(27) For original references, see: Michael, J. V. In *Advances in Chemical Kinetics and Dynamics*; Barker, J. R. Ed.; JAI: Greenwich, CT, 1992; Vol. I, pp 47−112.

(28) Michael, J. V.; Sutherland, J. W. *Int. J. Chem. Kinet.* **1986**, *18*, 409.

(29) Michael, J. V. *J. Chem. Phys.* **1989**, *90*, 189.

(30) Michael, J. V.; Fisher, J. R. In *Seventeenth International Symposium on Shock Waves and Shock Tubes*, AIP Conference Proceedings 208; Kim, Y. W., Ed.; American Institute of Physics: New York, 1990; pp 210−215.

(31) Su, M.-C.; Kumaran, S. S.; Lim, K. P.; Michael, J. V.; Wagner, A. F.; Dixon, D. A.; Kiefer, J. H.; DiFelice, J. *J. Phys. Chem.* **1996**, *100*, 15827.

(32) Kumaran, S. S.; Su, M.-C.; Lim, K. P.; Michael, J. V. *Proc. Combust. Inst.* **1996**, *26*, 605.

(33) Herbon, J. T.; Hanson, R. K.; Golden, D. M.; Bowman, C. T. *Proc. Combust. Inst.* **2002**, *29*, 1201.

(34) Ruscic, B.; Wagner, A. F.; Harding, L. B.; Asher, R. L.; Feller, D.; Dixon, D. A.; Peterson, K. A.; Song,Y.; Qian, X.; Ng, C. Y.; Liu, J.; Chen, W.; Schwenke, D. W. *J. Phys. Chem. A* **2002**, *106*, 2727.

(35) Krasnoperov, L. N.; Michael, J. V. *J. Phys. Chem. A* **2004**, *108*, 5643.

(36) Walter, D.; Grotheer, H.-H.; Davies, J. W.; Pilling, M. J.; Wagner, A. F. *Proc. Combust. Inst.* **1990**, *23*, 107. Hwang, S. M.; Rabinowitz, M. J.; Gardiner, W. C., Jr. *Chem. Phys. Lett.* **1993**, *205*, 157. Davidson, D. F.; Di Rosa, M. D.; Chang, A. Y.; Hanson, R. K.; Bowman, C. T. *Proc. Combust. Inst.* **1992**, *24*, 589. Davidson, D. F.; Hanson, R. K.; Bowman, C. T. *Int. J. Chem. Kinet.* **1995**, *27*, 305.

(37) Wooldridge, M. S.; Hanson, R. K.; Bowman, C. T. *Int. J. Chem. Kinet.* **1994**, *26*, 389.

(38) Krasnoperov, L. N.; Michael, J. V. *J. Phys. Chem. A* **2004**, *108*, 8317.

(39) Glaenzer, K.; Troe, J. *Ber. Bunsen-Ges. Phys. Chem.* **1974**, *78*, 182.

(40) Yamada, F.; Slagle, I. R.; Gutman, D. *Chem. Phys. Lett.* **1981**, *83*, 409.

(41) Biggs, P.; Canosa-Mas, C. E.; Fracheboud, J.-M.; Parr, A. D.; Shallcross, D. E.; Wayne, R. P.; Caralp, F. *J. Chem. Soc., Faraday Trans.* **1993**, *89*, 4163.

(42) Glarborg, P.; Bendtsen, A. B.; Miller, J. A. *Int. J. Chem. Kinet.* **1999**, *31*, 591.

(43) Wollenhaupt, M.; Crowley, J. N. *J. Phys. Chem. A* **2000**, *104*, 6429.

(44) Zaslonko, I. S.; Petrov, Yu. P.; Smirnov, V. N. *Kinet. Katal.* **1997**, *38*, 321.

(45) Zhang, Y. X.; Bauer, S. H. *J. Phys. Chem.* **1997**, *101*, 8717.

(46) Yamaguchi, Y.; Teng, Y.; Shimomura, S.; Tabata, K.; Suzuki, E. *J. Phys. Chem. A* **1999**, *103*, 8272.

(47) Cohen, N. *A Revised Model for Transition State Theory Calculations for Rate Coefficients of OH with Alkanes*; Aerospace Report No. ATR-90(7179)-1; March 1990.

(48) Leroy, G.; Sana, M.; Tinant, A. *Can. J. Chem.* **1985**, *63*, 1447.

(49) Gonzalez, C.; McDouall, J. J. W.; Schlegel, H. B. *J. Phys. Chem.* **1990**, *94*, 7467.

(50) Truong, T. N.; Truhlar, D. G. *J. Chem. Phys.* **1990**, *93*, 1761.

(51) Melissas, V. S.; Truhlar, D. G. *J. Chem. Phys.* **1993**, *99*, 1013, 3542.

(52) Dobbs, K. D.; Dixon, D. A.; Komornicki, A. *J. Chem. Phys.* **1993**, *98*, 8852.

(53) Hu, W.-P.; Liu, Y.-P.; Truhlar, D. G. *J. Chem. Soc., Faraday Trans. 2* **1994**, *90*, 1715.

(54) Nyman, G.; Clary, D. C. *J. Chem. Phys.* **1994**, *101*, 5756. Nyman, G. *Chem. Phys. Lett.* **1995**, *240*, 571.

(55) Basch, H.; Hoz, S. *J. Phys. Chem. A* **1997**, *101*, 4416.

(56) Skokov, S.; Wheeler, R. A. *Chem. Phys. Lett.* **1997**, *271*, 251.

(57) Schwartz, M.; Marshall, P.; Berry, R. J.; Ehlers, C. J.; Petersson, G. A. *J. Phys. Chem. A* **1998**, *102*, 10074.

(58) Korchowiec, J.; Kawahara, S.-i.; Matsumura, K.; Uchimaru, T.; Sugie, M. *J. Phys. Chem. A* **1999**, *103*, 3548.

(59) Espinosa-Garcia, J.; Corchado, J. C. *J. Chem. Phys.* **2000**, *112*, 5731.

(60) Masgrau, L.; Gonzalez-Lafont, A.; Lluch, J. *J. Chem. Phys.* **2001**, *114*, 2154; *115*, 4515; *Theor. Chem. Acc.* **2002**, *108*, 38.

(61) Kerkeni, B.; Clary, D. C. *J. Chem. Phys.* **2004**, *120*, 2308.